Experimental Validation for Microwave Based Real-time Monitoring for Microwave Ablation Treatment

Kazuki Kanazawa[1] and Shouhei Kidera[1]

***Abstract*— Microwave ablation (MWA) is one of the most promising treatment tool to achieve a minimal invasion for human body. For safety and effective ablation for cancerous tissue, the accurate and real-time imaging for a temporal evolution of the ablation zone is highly demanded. This paper assumes the microwave based MWA monitoring, and introduces the novel boundary reconstruction algorithm, which has been demonstrated to achieve a real-time, accurate and noise-robust characteristic. This paper also newly introduces the S_{11} based complex permittivity estimator, which is necessary for estimating the ablation boundary. The both finite difference time domain (FDTD) based 3-D numerical test and the experimental investigation demonstrate that the proposed method provides accurate and high-speed 3-D imaging for the ablation zone.**

I. Introduction

As a minimally invasive treatment for malignant tumor, microwave ablation (MWA) is highly recognized [1], which more quickly damage the tumors than the lower radio frequency (RF) based technique [2]. There are a great numbers of studies for assuming the liver tumor ablations [3], which demonstrates the effectiveness of MWA [3]. The above success brings us the driving force for applying the MWA to other types of cancer, e.g. kidney or breast tumors. In terms of breast cancer treatment, it is strongly demanded to avoid the removal of the whole or large part of breast, and the MWA is regarded as the most appropriate treatment tool, to avoid physical and mental burden for patient. Nonetheless, the MWA treatment requires accurate and real-time monitoring sensor to avoid the over-ablation for healthy cells. As such monitoring sensor, magnetic resonance imaging (MRI) and ultrasound based techniques have been demonstrated in a number of researches [4], [5]. However, the introduction cost of the MRI is much expensive and requires an electromagnetic shield, and its image could be contaminated by the effect of heating contrast agents [6]. The ultrasound based monitoring tool has some advantages in terms of low cost and portability, but microbubbles would contaminate a contrast image [7], as well as limited echogenic contrast between ablated and non-ablated tissue [8]. To overcomes the above difficulty, the microwave based monitoring is under the spotlight, because it has advantages for low cost, compactness and in compatibility with MWA equipment. Some studies have revealed that there was a significant decrease of complex permittivity for tissue in ablated state [9]. The above fact is basis for achieving accurate imaging using microwave signal, where its forward scattering component received at external antenna from interstitial MWA source is processed. As a traditional imaging approach, the tomographic inverse scattering algorithm has been developed, assuming the fairly homogeneous media, which is a reasonable assumption in liver tissue [10]. However, such kind of methods hardly achieves a real-time monitoring, and is not suitable for heterogeneous background, e.g. breast media.

To address with this issue, our research group has proposed a real-time and accurate imaging algorithms for the ablation zone evolution, such as the TDOA based method [11] or the waveform reconstruction based method [12]. In particular, the method [12] considers the drop of both real and imaginary parts of complex permittivity, and has been demonstrated that it offers accurate imaging in the situation that the lower impact, namely, lower decrease of temperature, is assumed. However, these methods requires a prior information of complex permittivity of the tissues for pre- and during ablation, which is the proximity of MWA probe. While the growing data revealing the relationship between the temperature and dielectric property of ablated tissues is available [13], its dielectric property is highly dependent of the subject.

As a solution for the above mentioned problem, this paper newly introduces the S_{11} parameter based estimation algorithm of complex permittivity of the tissue around the MWA probe. The 3-D FDTD numerical phantom, assuming the coaxial slot probe, and the experimental validation using the simple breast phantom demonstrates that our proposed method retains highly accurate boundary estimation for the ablation zone.

II. Observation Model

Figure 1 shows the observation model assuming the pre- and during microwave ablation. T denotes the elapsed time of the ablation, where $T = 0$ corresponds to a time pre-ablation and $T > 0$ corresponds to a time during the ablation. A single transmitter (shown as a hollow black circle in Fig. 1) is inserted into the tumor, which is located within the fibrograndular tissue, and multiple receivers are located surrounding the breast (shown as solid black circles in Fig. 1). The location of the source is defined as $\boldsymbol{r}_{\rm A}$, and the location of a representative receiver is defined as $\boldsymbol{r}_{\rm C}$. The received microwave signals pre-ablation (at $T = 0$) and during ablation (at the n-th temporal snapshot) are denoted by $s_{21}^{(0)}(\boldsymbol{r}_{\rm C}, t)$ and $s_{21}^{(n)}(\boldsymbol{r}_{\rm C}, t)$ respectively. The variable t denotes the signal recording time.

[1]Graduate school of Informatics and Engineering, The University of Electro-Communications, Japan kanazawa.kazuki@ems.cei.uec.ac.jp, kidera@uec.ac.jp

978-1-5386-1311-5/19/$31.00 ©2019 IEEE

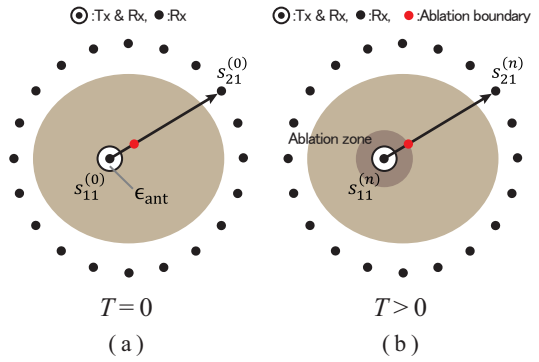

Fig. 1. Data acquisition configuration for MWA monitoring using the internal ablation antenna as the transmitter and an external array as the receivers. (a) Pre-ablation ($T = 0$). (b) During ablation ($T > 0$)

III. Method

A. Imaging Algorithm

Here, we present the imaging algorithm, which has been proposed in [12]. This algorithm focuses on the difference between pre- and during ablation. By using a prior estimation of complex permittivity drop of ablation zone, this algorithm determines the distance from the source to the ablation boundary. We briefly describe the methodology of this method as follows.

Here, let $\boldsymbol{r}_B$ as the ablation boundary point as marked in Fig. 1, and $R^{\mathrm{AB}} = |\boldsymbol{r}_{\mathrm{A}} - \boldsymbol{r}_{\mathrm{B}}|$ and $R^{\mathrm{BC}} = |\boldsymbol{r}_{\mathrm{B}} - \boldsymbol{r}_{\mathrm{C}}|$ are defined. On the assumptions that the same propagation model, used in the TDOA-based method, is valid and that signals propagate in a straight line, the pre- and during ablated signal in the angular-frequency domain can be expressed as:

$$S_{21}^{(0)}(\boldsymbol{r}_{\mathrm{C}}, \omega; R^{\mathrm{AB}}) = S_{\mathrm{src}}(\omega) e^{j(k_0(\omega)R^{\mathrm{AB}} + k(\omega)R^{\mathrm{BC}})} \quad (1)$$

$$S_{21}^{(n)}(\boldsymbol{r}_{\mathrm{C}}, \omega; R^{\mathrm{AB}}) = S_{\mathrm{src}}(\omega) e^{j(k_n(\omega)R^{\mathrm{AB}} + k(\omega)R^{\mathrm{BC}})}, \quad (2)$$

where $S_{21}^{(0)}(\boldsymbol{r}_{\mathrm{C}}, \omega; R^{\mathrm{AB}})$ and $S_{21}^{(n)}(\boldsymbol{r}_{\mathrm{C}}, \omega; R^{\mathrm{AB}})$ denote the received signals at pre- and during ablation state at n-th snapshot in the angular frequency domain. Here, the wavenumber at the n-th snapshot as $k_n(\omega)$ is expressed as:

$$k_n(\omega) = \beta_n(\omega) - j\alpha_n(\omega), \quad (3)$$

where $\alpha_n(\omega)$ and $\beta_n(\omega)$ are defined as:

$$\alpha_n(\omega) = \omega\sqrt{\mu\epsilon_n}\left[\frac{1}{2}\sqrt{1 + \frac{\sigma_n^2}{\omega^2\epsilon_n^2}} - \frac{1}{2}\right]^{\frac{1}{2}} \quad (4)$$

$$\beta_n(\omega) = \omega\sqrt{\mu\epsilon_n}\left[\frac{1}{2}\sqrt{1 + \frac{\sigma_n^2}{\omega^2\epsilon_n^2}} + \frac{1}{2}\right]^{\frac{1}{2}}. \quad (5)$$

Here, ϵ_n and σ_n are the relative permittivity and conductivity in the ablation state at the n-th snapshot, where R^{BC} denote the distance from $\boldsymbol{r}_{\mathrm{B}}$ to $\boldsymbol{r}_{\mathrm{C}}$ (receiver location). Using this model, the signal at the n-th snapshot ablation state is estimated as:

$$\hat{S}_{21}^{(n)}(\boldsymbol{r}_{\mathrm{C}}, \omega; R^{\mathrm{AB}}) = S_{21}^{(0)}(\boldsymbol{r}_{\mathrm{C}}, \omega) \cdot e^{-j(k_n(\omega) - k_0(\omega))R^{\mathrm{AB}}}. \quad (6)$$

Finally, the distance from the source to the ablation boundary at the n-th snapshot as R_n^{AB} calculated as:

$$\hat{R}_n^{\mathrm{AB}} = \arg\min_{R^{\mathrm{AB}}} \int |\hat{S}_{21}^{(n)}(\boldsymbol{r}_{\mathrm{C}}, \omega; R^{\mathrm{AB}}) - S_{21}^{(n)}(\boldsymbol{r}_{\mathrm{C}}, \omega)|^2 d\omega, \quad (7)$$

where $S_{21}^{(n)}(\boldsymbol{r}_{\mathrm{C}}, \omega)$ denotes the observation signal in the angular frequency domain at the n-th snapshot. Finally, the boundary point of ablation zone is obtained as $\boldsymbol{r}_{\mathrm{B}} = \hat{R}^{\mathrm{AB}}\boldsymbol{u} + \boldsymbol{r}_{\mathrm{A}}$, where $\boldsymbol{u}$ denotes a unit vector pointing from $\boldsymbol{r}_{\mathrm{A}}$ to $\boldsymbol{r}_{\mathrm{C}}$.

This method maintains the advantages described above, in that it only requires the ratio of the dielectric constants and the conductivity in ablated tissues to be known beforehand. In most clinical applications, the source is located inside the malignant tissue, and databases of the complex permittivity of various malignant tissues are available in the literature [11].

B. Complex permittivity estimation using S_{11} parameters

In the previous work [12], the complex permittivity of pre- and during ablation is determined by the data base, however, there should be variation of each subject, and these values should be directly determined by the measured signals. This paper then introduces the S_{11} parameter based complex permittivity estimation algorithm as follows.

At first, the following ratios are defined as

$$\rho_0 \equiv S_{11}^{(0)}(\omega)/S_{11}^{\mathrm{cal}}(\omega) \quad (8)$$

$$\rho_n \equiv S_{11}^{(n)}(\omega)/S_{11}^{\mathrm{cal}}(\omega), \quad (9)$$

where $S_{11}^{\mathrm{cal}}(\omega)$ denotes the calibrated S_{11} parameter using an object with a known dielectric property, i.e., ethanol or pure water. $S_{11}^{(0)}(\omega)$ and $S_{11}^{(n)}(\omega)$ denote the observed S_{11} parameters for pre- and during ablations, respectively. On the contrary, the S_{11} parameter is theoretically formulated as

$$S_{11}(\omega) = \frac{\sqrt{\mu(\omega)/\epsilon(\omega)} - \sqrt{\mu_{\mathrm{prob}}(\omega)/\epsilon_{\mathrm{prob}}(\omega)}}{\sqrt{\mu(\omega)/\epsilon(\omega)} + \sqrt{\mu_{\mathrm{prob}}(\omega)/\epsilon_{\mathrm{prob}}(\omega)}}, \quad (10)$$

where $\epsilon(\omega)$ and $\mu(\omega)$ are the complex permittivities and the permeability of ablated or calibrated medium. And $\epsilon_{\mathrm{prob}}(\omega)$ and $\mu_{\mathrm{prob}}(\omega)$ are the above parameters of the MWA probe. Then, the complex permittivity for pre- and during ablation is determined as

$$\epsilon_i(\omega) = \epsilon_{\mathrm{prob}}(\omega)\left[\frac{\frac{1}{\sqrt{\epsilon_{\mathrm{prob}}(\omega)}}(\rho_i - 1) - \frac{1}{\sqrt{\epsilon_{\mathrm{cal}}(\omega)}}(\rho_i + 1)}{\frac{1}{\sqrt{\epsilon_{\mathrm{cal}}(\omega)}}(\rho_i - 1) - \frac{1}{\sqrt{\epsilon_{\mathrm{prob}}(\omega)}}(\rho_i + 1)}\right]^{-2}, \quad (i = 0, n), \quad (11)$$

where n denotes the number of snapshots. $\epsilon_{\mathrm{prob}}(\omega)$ and $\epsilon_{\mathrm{cal}}(\omega)$ are the complex permittivities of the MWA probe and the calibration media. Finally, $\alpha(\omega)$ and $\beta(\omega)$ are determined by each complex permittivity, where the permeability μ is assumed to be the same as that in the air.

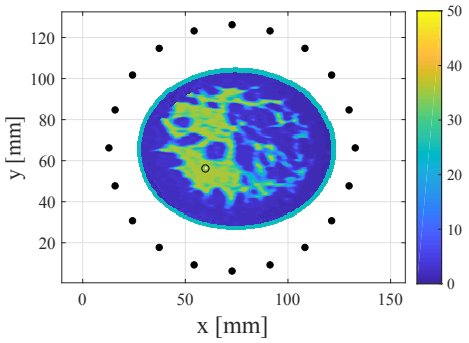

Fig. 2. 2-D numerical breast phantom and configuration. The colorbar displays the Debye parameter, $\Delta\varepsilon$ in Class 3 (heterogeneously dense) breast phantom. The hollow black circle denotes the location of the MWA probe while the solid circles denote the locations of the receiving antennas.

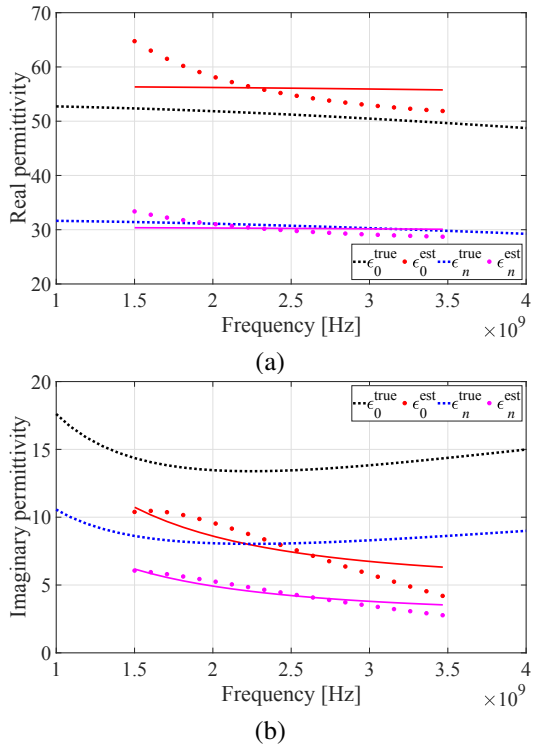

Fig. 3. Results of estimations of complex permittivity by the proposed method. Black and blue broken lines indicate the original Debye curve in the pre- and during ablation. Red and Purple dots denote the estimated values in the pre- and during ablation, and each solid lines are fitting curves by single-pole Debye model. (a): Real part of complex permittivity. (b): Imaginary part of complex permittivity.

As a notable feature of this method, it provides the change of complex permittivity without adding a specific probe or equipment, and offer a real-time monitoring for complex permittivity in the proximity of the MWA probe.

IV. 2-D Numerical Simulation Examples

A. Simulation model

This section describes the performance evaluation by the 2-D FDTD simulation, using the realistic breast phantoms as Class 3 "heterogeneously dense" (ID number: 062204), the dielectric profiles of which are derived from the MRI images [14]. These phantoms are available online at the University of Wisconsin repository [15]. The 2-D FDTD simulations with single-pole Debye model is used (in-house code provided by the cross-disciplinary electromagnetics laboratory at the University of Wisconsin, Madison). The frequency dependent complex permittivities for skin and breast tissues in the phantoms are also modeled by single-pole Debye models $\bar{\epsilon}(\omega) = \epsilon_\infty + \frac{\epsilon_s - \epsilon_\infty}{1+j\omega\tau_0} + \frac{\sigma}{j\omega\epsilon_0}$ over the frequency range from 0.1 to 5.0 GHz, as in [10]. Figure 2 shows the map of the Debye parameter $\Delta\epsilon$ of the Class 3 phantom. In this case, it is assumed that the MWA probe has a dielectric property with $\epsilon_\infty = 2.1, \Delta\epsilon = 0, \sigma = 0$ S/m, and is inserted into the central position of the ablation zone, shown as a hollow black circle in Fig. 2. The 20 receiving antennas, shown as solid black circles in Fig. 2, are located on a ring outside breast (immersed in air) with equal spacing. The situation without noise is assumed, to evaluate only the systematic error of the method.

The source current forms the Gaussian modulated pulse, with 2.45 GHz as the center frequency and a 1.9 GHz bandwidth. The cell size of the FDTD is 0.5 mm squares. In the ablation zone, there is the uniform decrease from that of pre-ablation state, namely, the dielectric map in the ablation zone are still heterogeneous. We have modeled the $\xi_\epsilon = \xi_\sigma = 0.6$ as the influence of ablation. This percentage range has been observed in ablations of bovine liver tissue [13] and human mastectomy specimens [9].

TABLE I

Estimation results of relative permittivity and conductivity of pre- and during ablation states

	Pre-ablation		During ablation	
	ϵ_0	σ_0 [S/m]	ϵ_n	σ_n [S/m]
Original	51.285	0.799	30.771	0.479
Estimated	56.100	0.813	30.252	0.473
Relative error	9.39%	1.75%	-1.69%	-1.25%

TABLE II

Estimated results for ablation factor (ξ)

	ξ_ϵ	ξ_σ
Original	0.6	0.6
Estimated	0.5385	0.5684
Relative error	-10.3%	-5.27%

B. Results and Discussions

Here, the ablation boundary that assumes 20 mm along the x-axis and 16 mm along the y-axis is reconstructed by using estimated complex permittivities in Sec. III-B. Figure 3 shows the results of the complex permittivity estimation for each frequency, where the ethanol medium $(\epsilon_\infty, \Delta\epsilon, \sigma) = (4.380, 20.615, 0.001$ S/m$)$ is used for the calculation of $S_{11}^{\mathrm{cal}}(\omega)$ [16]. Figure 3 shows that the estimation for complex permittivity is acceptable in terms of the real part of the permittivity, while there are significant errors in the imaginary part of permittivity, it is considered that the error is caused by the heterogeneity surrounding the MWA probe. Table I summarizes the original and estimation results of

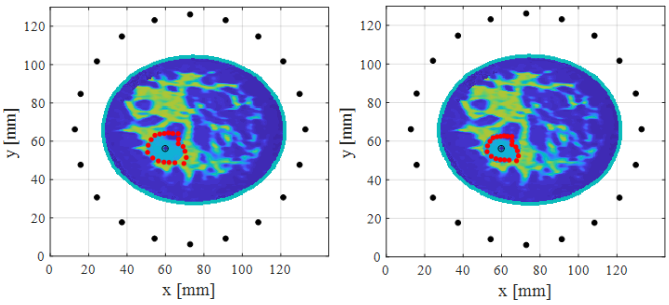

Fig. 4. Boundary reconstruction results using true and estimated complex permittivities, which shown as red points. The actual ablation zone is an ellipse with major radius (x-axis) of 10 mm and minor radius (y-axis) of 8 mm. (a): Estimated result using the original complex permittivities. (b): Estimated result using the estimated complex permittivities.

TABLE III

MATERIALS FOR SEMI-SOLID BREAST PHANTOMS

	Pre-ablation	During ablation
Rapeseed oil	130 ml	150 ml
Pure water	70 ml	50 ml
Neutral detergent	47 ml	35 ml
Agar	4.5 g	4.5 g

complex permittivity at 2.45 GHz. Table II also shows the error analysis for ablation impact denoted as ξ_ϵ and ξ_σ. These results demonstrate that our method achieves the accuracy for the complex permittivity estimation within 10 % relative errors.

Finally, we show the imaging performance of the method [12] using the estimated complex permittivity. Figure 4 indicates the results of the reconstruction for the ablation zone using the original and estimated complex permittivity. The median errors of the ablation zone estimation are 0.691 mm , where the permittivity is given, and 1.832 mm , where the permittivity is estimated by our method, respectively. While the results obtained by our method become slightly worse compared with that in the ideal situation, it is considered that the accuracy for ablation zone estimation is acceptable, comparing the whole size of the ablation zone. The computational time required for the imaging is within 0.3 sec using the Intel Xeon CPU E5-1620 v2 3.7 GHz with 16 GB RAM.

V. EXPERIMENTAL VALIDATION

A. Observation Setup and Breast Phantom

This section describes the experimental validation using the simplified breast phantom model. Figure 5 shows the measurement setup with the breast phantom. We introduce the single slot coaxial probe with 2.2 mm diameter as ablation probe, where its S_{11} characteristic is adjusted to the dielectric property with $\epsilon = 42$, which corresponds to that of the typical fibroglandular tissue. The center frequency of this antenna is designed at 2.45 GHz. Vector network analyzer (TTR500, Oregon, Tektronix, Inc.) is used for S_{11} and S_{21} data acquisition, where the frequency is swept from 0.01 GHz to 5.01 GHz with 6.25 MHz sampling. The RF amplifier with 15 dBm (87405C, California, Keysight

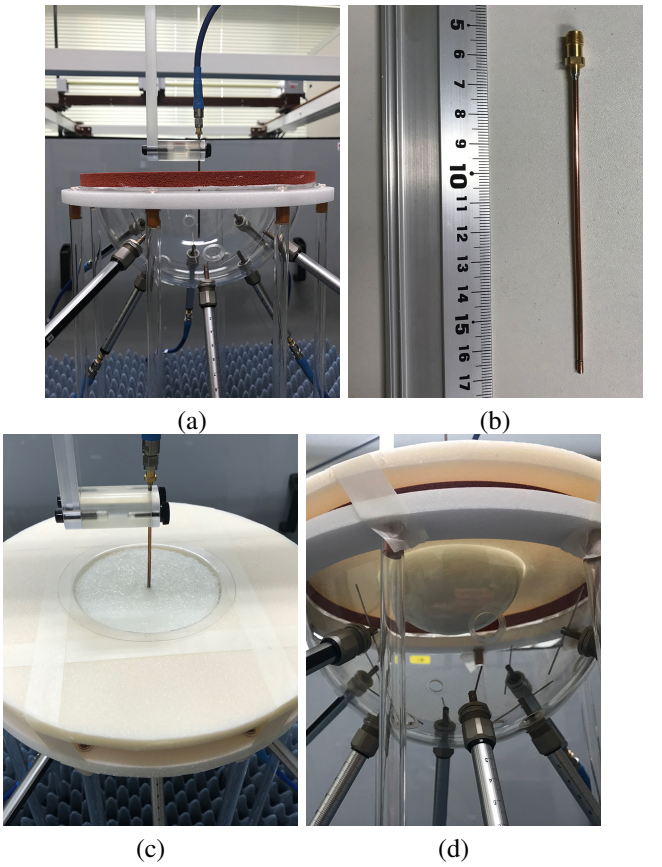

Fig. 5. Measurement setup and phantom. (a): Hemisphere-shaped measurement cup with 8 dipole receivers. (b): Coaxial slot antenna for MWA probe. (c), (d): Simplified breast phantom and measurement state.

TABLE IV

ESTIMATED RELATIVE PERMITTIVITY AND CONDUCTIVITY

Pre-ablation		During ablation		ξ_ϵ	ξ_σ
ϵ_0	σ_0 [S/m]	ϵ_n	σ_n [S/m]		
21.64	0.6878	12.51	0.3460	0.578	0.503

Technologies, Inc.) is used to amplify the transmitting signal power. The 8 dipole receives with 24 mm length are arranged on the hemisphered cup with acrylic resin, the radius of which is 90 mm. We prepare the two semi-solid breast phantoms having different dielectric property, the radius of which is 50 mm, to model the pre- and during ablation state in the breast. For simplicity, these two phantom have a homogeneous dielectric property, which are made by the blend of the materials indicated in Table III.

B. Results and Discussions

Table IV shows the measured relative permivitivities and conductivities of the phantoms modeling the pre- and during ablation state. Note that, to focus on the performance evaluation of ablation zone monitoring by the method [12], the above permittivity and conductivity are measured by the commercial equipment and software (DSP16, DMP-60, KEYCOM Corp.). Figure 6 illustrates the result of ablation zone estimation using the method [12]. The median of errors is 2.48 mm in this case, and we confirm that

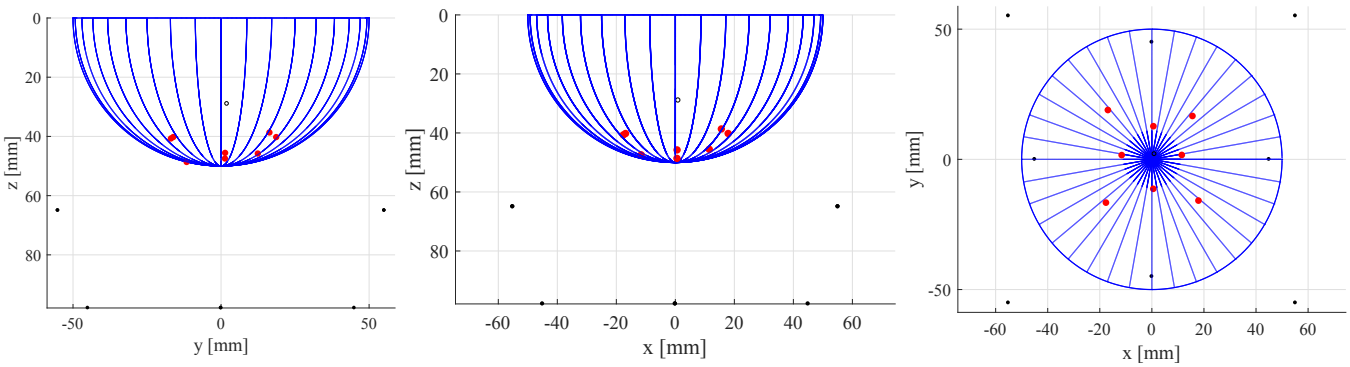

Fig. 6. Estimated boundary points shown by the red circles using the measured data, where the actual ablation boundary is expressed as blue solid lines and the center of the MWA probe is denoted as the hollow circle. (a)x-plane projection (b) y-plane projection (c) z-plane projection.

our proposed method can reconstruct the ablation boundary accurately. Furthermore, the computational time required for the imaging is within 3 sec using the Intel Xeon CPU E5-1620 v2 3.7 GHz with 16 GB RAM. It is considered that the errors for boundary estimation is caused by the interference of signal leaked from the ablation probe.

VI. Conclusion

This paper proposed the complex permittivity estimation using S_{11} parameters for accurate and real-time microwave ablation monitoring scenario, and validated our previous method through the experimental measurement using the simplified ablation phantom. In the 2-D FDTD simulation, the results demonstrate that the accuracy of the complex permittivity by S_{11} parameter is sufficient to obtain the accurate reconstruction of ablation zone. In addition, the experimental validation, we demonstrated that our method [12] provides accurate boundary extraction with a considerably lower processing time. It is our future work to evaluate our method using the real ablated tissues.

ACKNOWLEDGMENT

This research and development work was supported by the MIC/SCOPE #162103102.

References

[1] A. Rosen, M. A. Stuchly, and A. V. Vorst, Applications of RF/Microwaves in Medicine, *IEEE Transactions on Microwave Theory and Techniques*, Vol. 50, Mar. 2002.

[2] G. Carrafiello, D. Lagana, M. Mangini, F. Fontana, G. Dionigi, L. Boni, F. Rovera, S. Cuffari and C. Fugazzola, Microwave tumors ablation: Principles, clinical applications and review of preliminary experiences, *Int. J. Surg.*, S65-9, Dec. 2008.

[3] R. C. G. Martin, C. R. Scoggins and K. M. McMasters, Safety and efficacy of microwave ablation of hepatic tumours: a prospective review of a 5-year experience, *Ann. Surg. Oncol.*, vol. 17, pp. 171-178, Jan. 2010

[4] Y. Kurumi, T. Tani, S. Naka, H. Shiomi, T. Shimizu, H. Abe, Y. Endo and S. Morikawa, MR-guided microwave ablation for malignancies, *International Journal of Clinical Oncology*, vol. 12, no. 2, pp. 85-93, Apr. 2007.

[5] S. Huang, J. Yu and P. Liang, Percutaneous Microwave Ablation for Liver Tumors Adjacent to Large Vessels, in *Microwave Ablation Treatment of Solid Tumors*, P. Liang, X. Yu and J. Yu, Eds. Heidelberg: Springer, 2015.

[6] L. G. Merckel, L. W. Bartels, M. O. Kohler, H. J. G. D. van den Bongard, R. Deckers, W. Mali, C. Binkert, C. T. Moonen, K G. A. Gilhuijs, and M. A. A. J. van den Bosch, MR-guided high-intensity focused ultrasound ablation of breast cancer with a dedicated breast platform, *Cardiovasc. Intervent. Radiol.*, vol. 36, no. 2, pp. 292-301. Apr. 2013.

[7] Correa-Gallego, M. D., A. M. Karkar, S. Monette, P. C. Ezell, W. R. Jarnagin, and T. P. Kingham, Intraoperative ultrasound and tissue elastography measurements do not predict the size of hepatic microwave ablations, *Acad. Radiol.*, vol. 21, no. 1. pp. 72-78, Jan. 2014.

[8] W. Yang, M. Alexander, N. Rubert, A. Ingle, M. Lubner, T. Ziemlewicz, J. L. Hinshaw, F. T. Lee Jr, J. A. Zagzebski, T. Varghese, Monitoring Microwave Ablation for Liver Tumors with Electrode Displacement Strain Imaging, *Proc. of 2014 IEEE International Ultrasonics Symposium (IUS)*, Sept. 2014.

[9] R. O. Mays, L. M. Neira, A. Schulman, J. Harter, L. G. Wilke, N. Behdad, and S. C. Hagness, A pilot study of microwave ablation in ex vivo human breast tissue, *Proc. of USNC/URSI National Radio Science Meeting*, Puerto Rico, June 2016.

[10] O. M. Bucci, M. Cavagnaro, L. Crocco, V. Lopresto and R. Scapaticci, Microwave Ablation Monitoring via Microwave Tomography: a Numerical Feasibility Assessment, *Proc. of 2016 10th European Conference on Antennas and Propagation*, 2016.

[11] S. Kidera, L. M. Neira, B. D. V. Veen, and S. C. Hagness, TDOA-based microwave imaging algorithm for real-time microwave ablation monitoring, *International Journal of Microwave and Wireless Technologies*, November, 2017.

[12] K. Kanazawa and S. Kidera, Waveform Matching Based Real-time Ablation Monitoring for Microwave Breast Cancer Ablation, *Proc. of 2018 12th European Conference on Antennas and Propagation*, Apr., 2016.

[13] V. Lopresto, R. Pinto, G. A Lovisolo, and M. Cavagnaro, Changes in the dielectric properties of ex vivo bovine liver during microwave thermal ablation at 2.45 GHz, *Phys. Med. Biol.*, vol. 57, pp. 2309 -2327, 2012.

[14] M. Lazebnik, D. Popovic, L. McCartney, C. B.Watkins, M. J. Lindstrom, J. Harter, S. Sewall, T. Ogilvie, A. Magliocco, T. M. Breslin, W. Temple, D. Mew, J. H. Booske, M. Okoniewski, and S. C. Hagness, A large-scale study of the ultrawideband microwave dielectric properties of normal, benign, and malignant breast tissues obtained from cancer surgeries, *Physics in Medicine and Biology*, vol. 52, pp. 6093-6115, 2007.

[15] University of Wisconsin Cross-Disciplinary Electromagnetics Laboratory (UWCEM), Numerical breast phantom repository [Online]. Available: http://uwcem.ece.wisc.edu, accessed on: October 2, 2017.

[16] A. P. Gregory and R. N. Clarke, Tables of the complex permittivity of dielectric reference liquids at frequencies up to 5 GHz, *NPL Report MAT 23*, jan. 2012.

[17] R. Ortega-Palacios, L. Leija, A. Vera, M. F. J. Cepeda, Measurement of breast - tumor phantom dielectric properties for microwave breast cancer treatment evaluation, *Computing Science and Automatic Control (CCE 2010)*, September, 2010